PAPER

Spallation reactions induced by 4.4 GeV deuterons on lead isotopes

IOP Publishing Journal of Physics G: Nuclear and Particle Physics
J. Phys. G: Nucl. Part. Phys. **46** (2019) 095103 (23pp) https://doi.org/10.1088/1361-6471/ab2bce

Spallation reactions induced by 4.4 GeV deuterons on lead isotopes

A R Balabekyan[1], G S Karapetyan[2], N A Demekhina[3], S V Gaginyan[1,7], J R Drnoyan[4], V I Zhemenik[4], J Adam[4], L Zavorka[4], A A Solnyshkin[4], V M Tsoupko-Sitnikov[4], J Khushvaktov[4], V Pronskikh[4,5], V M Zhamkochyan[1], V Guimarães[6] and A Deppman[6]

[1] Yerevan State University, A. Manoogian, 1, 025, Yerevan, Armenia
[2] Centro de Ciências Naturais e Humanas, Universidade Federal do ABC, 09210-580, Santo Andre, SP, Brazil
[3] Yerevan Physics Institute, Alikhanyan Brothers 2, Yerevan 0036, Armenia
[4] Joint Institute for Nuclear Research (JINR), Laboratory of Nuclear Problems (LNP), Joliot-Curie 6, Dubna 141980, Moscow, Russia
[5] Fermi National Accelerator Laboratory, Batavia, United States of America
[6] Instituto de Física Universidade de São Paulo, Rua do Matão 1371, 05508-090 São Paulo, SP, Brazil

E-mail: balabekyan@ysu.am, gayane.karapetyan@ufabc.edu.br, nina@mail.yerphi.am, susgaginyan@ysu.am, drnoyan@yandex.ru, laser@jinr.ru, iadam@jinr.ru, zavorluk@fjfi.cvut.cz, soln@jinr.ru, vtsoupko@jinr.ru, khushvaktov@mail.ru, Vitali.Pronskikh@jinr.ru, vzh@mail.yerphi.am, valdirg@if.usp.br and deppman@if.usp.br

Received 11 October 2018, revised 20 June 2019
Accepted for publication 21 June 2019
Published 7 August 2019

Abstract

Independent and cumulative production cross sections for radioactive nuclear fragments from the deuteron-irradiation of isotopically enriched lead (^{204}Pb, ^{206}Pb, ^{207}Pb, and ^{208}Pb) targets were obtained for the first time. The experiment has been performed with a 4.4 GeV deuteron beam from the Nuclotron of the Laboratory of High Energy Physics (LHE), Joint Institute for Nuclear Research (JINR) at Dubna. The production cross sections of target fragments were determined by off-line γ-ray spectroscopy. Charge dispersion and mass-yield distributions were deduced from these data. The results are discussed in terms of the relative importance of different reaction mechanisms (evaporation–spallation, fission and multifragmentation). Comparison of our results with the data from the reaction induced by protons of about the same kinetic energy per nucleon, has been performed. The coexistence of the different

[7] Author to whom correspondence should be addressed.

decay modes in the formation of the reaction residues, such as spallation, fission and multifragmentation is suggested.

Keywords: evaporation–spallation reactions, fission, multifragmentation, off-line gamma-spectroscopy method

(Some figures may appear in colour only in the online journal)

1. Introduction

High energy nuclear reactions play an important role in a large variety of domains, ranging from fundamental astrophysics to spallation sources for different applications. The interaction of a high energy (above a few hundreds of MeV) light particle on a nucleus leads to the emission of a large number of particles and reaction residues, whose production cross sections have the highest importance for radiotoxicity, activity and chemical corrosion problems. Disintegration of heavy targets usually can be described by two stages: intra-nuclear cascade and de-excitation. First, the nucleon–nucleon interactions in the nucleus lead to an excited pre-fragment. Secondly, the pre-fragment de-excites by emitting nuclides, nucleons and γ-rays, and/or by fission or fragmentation. The rest of the energy after the first stage is equally distributed among nucleons in the nucleus which is left in a highly excited state. A competitive process to evaporation is fission.

The mass distribution of the fragments produced in the disintegration of heavy- and medium-mass nuclei at various excitation energies exhibits very different and interesting shapes. At the excitation energy region of 1–3 MeV per nucleon, a U-shape distribution of reaction products is usually observed. This U-shape distribution contains one big residual fragment and a few nucleons and lightest clusters. In this case, the big fragment can undergo fission during the secondary de-excitation. At higher excitations, i.e. more than 3–4 MeV per nucleon, we enter into the so-called nuclear liquid–gas phase transition region, where the statistical equilibrium is assumed when a hot nucleus is expanded to the low density region. When this matter enters the region of subsaturation densities, it becomes unstable to density fluctuations and breaks up into many fragments in the multifragmentation process. The most comprehensive review, that has been devoted to the study of such a transition of the excited nuclear matter, is that by Borderie and Rivet [1], where the phenomenon of the multi-fragmentation has been deeply investigated by using the powerful 4π multidetectors of INDRA array [2] operating at GANIL and GSI. The authors have collected the latest results concerning the fragment formation mechanism and primary fragment excitation energy as well as made the detailed analysis and instructive comparisons with dynamical and statistical models.

The spallation reactions have gained growing interest in recent years. In fact, they can be used as intensive neutron sources in accelerator-driven subcritical reactor systems and in physical and technological researches. Designing the accelerator-driven subcritical systems (ADS facilities) requires that the cross sections of various reaction-produced nuclei should be known within a sufficient accuracy that would make it possible to predict the number of radioactive isotopes produced in a target. Data on Pb isotopes are of particular importance, since such elements are regarded as the best target material in most of the latest conceptual designs of ADS facilities [3]. Therefore, the excitation functions of the residual product cross sections in ^{204}Pb, ^{206}Pb, ^{207}Pb, and ^{208}Pb are extremely desirable to be measured in detail.

In the past, cross-section measurements for different lead isotopes have been performed for reactions with protons as a projectile. The most comprehensive set of data is that of Yu. E. Titarenko *et al* [4, 5], about the cross sections of residual nuclei produced in thin Pb targets irradiated by 40–2600 MeV protons. In that work the cross sections of a number of target products have been measured by direct counting using the semiconductor γ-ray spectrometry. The predictive powers of different models have been analyzed and proven to vary significantly. The available experimental data on fission cross sections for lead isotopes are compiled in [6], where they were used to develop a phenomenological systematics of the proton-induced fission cross section for energies up to 10 GeV.

High energy reactions induced by deuterons have the particularity that, due to the low binding energy of the deuteron (2.22 MeV), the reaction can proceed with the deuteron as a whole nucleus or as two non-interacting nucleons (proton plus neutron). A survey on the literature displays that there is a considerable lack of experimental data for the deuteron interaction with lead targets. The deuteron-induced reactions have been rarely explored in the energy range above 1–2 GeV. One of such experiments has been performed at the energy 2.1 GeV, where the cross sections for binary and ternary fission were measured by using plastic detectors [7]. In another work the charge-pickup cross sections and velocity distributions have been measured in the reactions of 1 *A* GeV ^{208}Pb with deuteron target [8]. In order to obtain high-precision experimental data on mass, atomic number, and momentum distributions of reaction residues, the authors made use of a high-resolution magnetic spectrometer. Little attention has been directed toward the measurements of entire spectra of the reaction product mass number, extending from light mass fragments up to near-target products except of the investigation of Enqvist *et al* [9]. In this work, the production cross sections and the kinematical properties of primary residual nuclei for the elements from titanium ($Z = 22$) to lead ($Z = 82$) have been measured in the reaction ^{208}Pb (1 *A* GeV) + *d* using the fragment separator FRS at GSI, Darmstadt.

Due to lack of data, it is important, therefore, to obtain complete experimental information on deuteron-induced production at higher energies. Experimental information, using deuteron as a projectile at high energies, as well as the observation of reaction products in a wide range of reaction product mass numbers, are required in order to understand more completely the dominant nuclear reaction mechanisms. The absence of experimental data on deuterons above an energy of several GeV has motivated us to measure fragment production cross sections and to determine the distribution in Z and A of the residual nuclei resulting from the interaction for different reaction channels such as fragmentation/fission/spallation of different lead isotopes.

The investigation of medium-mass target disintegration is important for the subcritical nuclear reactor driven by an external spallation neutron source (ADS) in order to produce fissile materials as well as for the estimation of efficiencies of various modes of radioactive waste transmutation [10]. Data on spallation reaction cross sections are used in nuclear physics basic research to provide information on the evolution of different mechanisms of nuclear reactions at GeV energies. Particularly, the knowledge of the cross sections on the lead isotopes and the multiplicity of emitted neutrons can stimulate the development of experimental and theoretical investigations concerning spallation and fission of heavy nuclei.

The aim of this study is the determination of the independent and cumulative cross sections of residual radioactive nuclei in high-energy deuteron-irradiated targets made of isotopically enriched lead (^{204}Pb, ^{206}Pb, ^{207}Pb, and ^{208}Pb). The results of this experiment provide a complete survey on the residues production, charge- and mass-yield distributions for a wide mass range of fragments at the energy 4.4 GeV for the first time. By comparing the new data with recent empirical systematics, the remarkable progress in the experimental

Table 1. Main characteristics of the targets.

Target	Size (cm^2)	Weight (g)	Thickness (μm)
^{204}Pb	1.05 × 0.72	0.0625	30
^{206}Pb	1.85 × 3.15	0.325	50
^{207}Pb	1.95 × 2.90	0.35	53
^{208}Pb	1.8 × 1.6	0.193	55

knowledge on spallation–fission reactions will be demonstrated. The present work represents the sequel of a systematic investigation of deuteron interaction with different targets that we have been carrying out in Joint Institute for Nuclear Research (JINR), Dubna. In the previous work on 4.4 GeV deuteron interaction on ^{197}Au [11], the kinematics analysis of the fragments charge- and mass-distributions allowed us to suggest one-nucleon collision character in the interaction, with high impact parameter. In our work we used a hard sphere model [12] to specify the role of the projectile and different processes such as spallation/fission involved in the reaction. However, investigation based on the advanced and capable models, which can describe the whole range of the reaction products, is needed in the future to understand the reaction mechanism.

2. Experimental procedure

A beam of 4.4 GeV deuterons from the Nuclotron of the VBLHEP, JINR was used to irradiate enriched lead targets. The targets were metal foils whose main characteristics are presented in table 1. The following metal samples from enriched lead were used: ^{208}Pb (98.7%), ^{206}Pb (87.9%), ^{207}Pb (90.4%), ^{204}Pb (51%). In the case of ^{204}Pb, the rest 49% of the target composition was the following: ^{208}Pb (25.0%), ^{206}Pb (12.0%), ^{207}Pb (12.0%). $^{206,\ 207,\ 208}$Pb targets had a rectangular shape, and ^{204}Pb target had a triangular shape. Each target was sandwiched by a pair of 38 μm Al foils with the same size. All foils were piled up together and aligned perpendicular to the beam direction. The reaction ^{27}Al $(d, 3p2n)^{24}$Na with a cross section of 15.25 ± 1.5 mb [13] was used for beam monitoring for each target separately in order to get the intensities in each case. As the targets had a different size, the obtained beam intensities were also different even though they were irradiated simultaneously.

The total irradiation time for all targets was 73.37 h at ion beam intensity of about $(2.39 \pm 0.3) \times 10^7$ deuterons $cm^{-2}\,s^{-1}$) for ^{204}Pb, $(4.91 \pm 0.5) \times 10^7$ deuterons $cm^{-2}\,s^{-1}$ for ^{206}Pb, $(4.46 \pm 0.5) \times 10^7$ deuterons $cm^{-2}\,s^{-1}$ for ^{207}Pb, $(4.56 \pm 0.5) \times 10^7$ deuterons $cm^{-1}\,s^{-1}$ for ^{208}Pb.

The γ-rays from the decay of residual nuclei formed in the target were measured off-line with four High purity Germanium (HpGe) detectors with 28% relative efficiency and an energy resolution of 2 keV (^{60}Co at 1332 keV). The energy-dependent efficiencies of the HpGe detectors were measured with standard calibration sources of ^{54}Mn, $^{57;60}$Co, ^{137}Cs, ^{154}Eu, ^{152}Eu, and ^{133}Ba. The γ-spectra were evaluated with the code package DEIMOS32 [14]. The residual radioactive nuclei were identified by the energy and intensity of characteristic γ-lines and by the respective half-lives of the nucleus.

Nuclear properties used for the identification were taken from literature [15]. The half-lives of identified isotopes were within the range of 15 min and 1 year. The errors in the determined cross sections depended on the following factors: the statistical uncertainties in the experimental results ($\leqslant$2%–3%), the errors in determining the detector (energy-

dependent) efficiency ($\leqslant$10%), and the uncertainties in half-lives, γ-ray intensities and absorption coefficients in nuclear data tables ($\leqslant$3%).

In the case of independent production of a nuclide (I), when a given isotope is made directly in the reaction, and the cumulative production (C) over time due to either β^+- or β^--decays, when the lifetimes of the parent nuclei are very short in comparison to lifetime of the product and one cannot be separated from the another, the cross section can be determined by using the following equation:

$$\sigma = \frac{\Delta N\ \lambda}{N_d\ N_n\ k\ \epsilon\ \eta(1\ -\ \exp(-\lambda t_1))\exp(-\lambda t_2)(1\ -\ \exp(-\lambda t_3))}, \tag{1}$$

where σ is the cross section of the reaction fragment production (mb); ΔN is the area under the photoabsorption peak; N_d is the deuteron beam intensity (min^{-1}); N_n is the number of target nuclei (in 1 cm^{-2} units); t_1 is the irradiation time; t_2 is the time of exposure between the end of the irradiation and the beginning of the measurement; t_3 is the measurement time; λ is the decay constant (min^{-1}); η is the relative intensity (%) of γ-transitions; k is the total coefficient of γ-ray absorption, which includes the absorption in the target, in the air zone between the target and the detector as well as the detector shield, and ϵ is the γ-ray detection efficiency. During the calculation of the production cross section from the ^{204}Pb target, the obtained cross section was corrected according to the fraction of the corresponding contribution to the cross section from other targets.

If the formation cross section of the parent isotope is known from experimental data, or if it can be estimated on the basis of other sources, the independent cross sections of daughter nuclei can be calculated using the relation [16]:

$$\begin{aligned}\sigma_B = &\frac{\lambda_B}{(1\ -\ \exp(-\lambda_B t_1))\exp(-\lambda_B t_2)(\ 1\ -\ \exp(-\lambda_B t_3))}\\ &\times\left[\frac{\Delta N_{AB}}{N_d\ N_n\ k\ \epsilon\ \eta}\ -\ \sigma_A f_{AB}\ \frac{\lambda_A\ \lambda_B}{\lambda_B\ -\ \lambda_A}\right.\\ &\times\left(\frac{(1\ -\ \exp(-\lambda_A t_1))\exp(-\lambda_A t_2)(1\ -\ \exp(-\lambda_A t_3))}{\lambda_A^2}\right.\\ &\left.\left.-\ \frac{(1\ -\ \exp(-\lambda_B t_1))\exp(-\lambda_B t_2)(1\ -\ \exp(-\lambda_B t_3))}{\lambda_B^2}\right)\right],\end{aligned} \tag{2}$$

where the subscripts A and B label variables referring to the parent and the daughter nucleus, respectively; the coefficient f_{AB} specifies the fraction of A nuclei decaying to a B nucleus ($f_{AB} = 1$, when the contribution from the β-decay corresponds 100%); and $(\Delta N)_{AB}$ is the total photopeak area associated with the decays of the daughter and parent isotopes. The effect of the precursor can be negligible in some limiting cases: where the half-life of the parent nucleus is very long, or in the case where its contribution is very small. It should be mentioned that the use of induced-activity method imposes several restrictions on the registration of the reaction products. For example, it is impossible to measure stable and very long-lived or very short-lived isotopes.

3. Results and discussion

In the reactions of ^{204}Pb, ^{206}Pb, ^{207}Pb, and ^{208}Pb induced by 4.4 GeV deuterons, the production cross sections were determined for 72, 87, 87 and 88 target fragments, respectively.

Table 2. Production cross sections for fragments formed by the interaction of 4.4 GeV deuterons with different lead isotopes. Independent and cumulative cross sections are indicated by (*I*) and (*C*), respectively.

Nuclide	Type	σ, mb			
		^{204}Pb	^{206}Pb	^{207}Pb	^{208}Pb
^{22}Na	C	3.47 ± 0.31	0.60 ± 0.05	0.68 ± 0.07	0.67 ± 0.07
^{24}Na	C	5.55 ± 0.58	6.11 ± 0.13	7.18 ± 0.80	9.52 ± 0.13
^{43}K	C	1.14 ± 0.11	2.0 ± 0.2	1.93 ± 0.19	2.52 ± 0.25
^{46}Sc	I	1.58 ± 0.32	2.27 ± 0.38	2.59 ± 0.28	3.17 ± 0.38
^{48}Sc	C	0.60 ± 0.10	1.04 ± 0.20	1.09 ± 0.10	1.75 ± 0.20
^{48}V	C	0.59 ± 0.05	0.56 ± 0.02	0.59 ± 0.06	0.70 ± 0.07
^{54}Mn	I	1.55 ± 0.25	1.31 ± 0.10	1.65 ± 0.10	1.51 ± 0.10
^{58}Co	I	2.20 ± 0.50	2.10 ± 0.20	2.23 ± 0.30	2.82 ± 0.38
^{59}Fe	C	—	1.33 ± 0.06	1.48 ± 0.31	1.76 ± 0.25
^{74}As	I	1.98 ± 0.13	1.8 ± 0.2	2.03 ± 0.20	2.38 ± 0.25
^{75}Se	C	—	2.09 ± 0.51	2.33 ± 0.42	2.33 ± 0.30
^{76}Kr	C	$\leqslant$0.37	$\leqslant$0.26	$\leqslant$0.36	$\leqslant$1.86
^{83}Rb	C	6.24 ± 1.16	5.67 ± 0.76	5.81 ± 0.51	7.07 ± 0.90
^{84}Rb	I	3.12 ± 0.51	3.27 ± 0.63	3.29 ± 0.03	4.24 ± 0.13
^{85}Sr	C	6.89 ± 0.65	5.65 ± 0.38	5.70 ± 0.30	7.02 ± 0.70
^{86}Zr	C	0.85 ± 0.04	1.92 ± 0.20	1.19 ± 0.30	2.82 ± 0.30
^{87}Y	C	4.66 ± 0.46	5.05 ± 0.50	5.91 ± 0.50	6.67 ± 0.80
^{88}Y	C	2.88 ± 0.39	3.65 ± 0.63	4.20 ± 0.70	4.35 ± 0.70
^{89}Zr	C	3.83 ± 0.50	4.31 ± 0.10	4.70 ± 0.30	5.49 ± 0.30
^{95m}Nb	I	0.42 ± 0.04	0.58 ± 0.08	0.48 ± 0.09	0.52 ± 0.06
^{95}Nb	C	1.63 ± 0.19	1.69 ± 0.16	1.95 ± 0.28	2.19 ± 0.21
^{95}Tc	C	2.16 ± 0.19	3.92 ± 0.13	—	6.27 ± 0.70
^{95m}Tc	C	—	1.13 ± 0.11	1.17 ± 0.12	2.26 ± 0.23
^{99m}Rh	C	—	1.91 ± 0.32	2.37 ± 0.62	2.12 ± 0.61
^{103}Ru	C	1.23 ± 0.12	1.35 ± 0.14	1.43 ± 0.14	1.63 ± 0.16
^{105}Ag	C	—	3.8 ± 0.5	1.8 ± 0.2	1.3 ± 0.1
^{106m}Ag	I	—	0.77 ± 0.10	1.11 ± 0.20	1.15 ± 0.12
^{113}Sn	C	8.05 ± 0.97	8.0 ± 1.3	9.48 ± 0.90	11.2 ± 1.2
^{119m}Te	C	1.17 ± 0.31	1.11 ± 0.20	1.27 ± 0.20	1.56 ± 0.30
^{121}Te	C	5.34 ± 0.51	5.61 ± 0.51	6.4 ± 1.3	7.59 ± 0.51
^{126}Sb	I	—	0.13 ± 0.04	0.20 ± 0.04	0.23 ± 0.03
^{127}Xe	C	5.09 ± 0.97	5.51 ± 0.63	5.78 ± 0.85	8.19 ± 0.80
^{132}Cs	I	0.79 ± 0.15	1.35 ± 0.30	1.45 ± 0.40	1.67 ± 0.30
^{139}Ce	C	—	8.68 ± 0.76	8.28 ± 0.76	10.3 ± 1.0
^{143}Pm	C	6.99 ± 0.70	7.46 ± 0.70	8.34 ± 0.50	10.9 ± 2.0
^{144}Pm	I	—	0.51 ± 0.05	0.40 ± 0.05	0.59 ± 0.06
^{145}Eu	C	4.56 ± 0.56	6.83 ± 0.90	7.69 ± 0.77	8.9 ± 1.2
^{146}Gd	C	4.24 ± 0.39	4.05 ± 0.63	4.96 ± 0.50	5.63 ± 0.50
^{147}Eu	C	12.7 ± 1.2	13.23 ± 1.40	14.7 ± 1.5	16.9 ± 1.8
^{148}Eu	I	—	0.37 ± 0.05	0.44 ± 0.09	0.56 ± 0.06
^{149}Gd	C	5.63 ± 0.52	6.4 ± 1.0	6.8 ± 1.3	8.6 ± 1.1
^{153}Gd	C	—	4.51 ± 0.38	5.50 ± 0.60	7.4 ± 2.0
^{155}Tb	C	6.7 ± 1.0	6.53 ± 0.50	7.5 ± 0.7	9.1 ± 0.9
^{155}Dy	C	6.37 ± 0.51	7.45 ± 0.90	8.52 ± 0.60	10.7 ± 0.9
^{165}Tm	C	6.24 ± 0.62	7.13 ± 0.71	10.5 ± 1.0	11.4 ± 1.1
^{167}Tm	C	6.22 ± 0.31	10.1 ± 1.1	10.4 ± 1.0	13.4 ± 1.3

Table 2. (Continued.)

Nuclide	Type	σ, mb			
		^{204}Pb	^{206}Pb	^{207}Pb	^{208}Pb
^{169}Lu	C	5.92 ± 0.87	5.55 ± 0.60	6.65 ± 0.60	7.9 ± 0.9
^{169}Yb	I	6.32 ± 0.97	6.56 ± 0.89	7.13 ± 0.70	10.1 ± 1.1
^{170}Hf	C	9.8 ± 1.0	6.12 ± 0.70	7.1 ± 1.3	7.84 ± 0.90
^{171}Lu	C	10.6 ± 1.1	11.5 ± 1.2	12.9 ± 1.3	15.6 ± 1.6
^{173}Hf	C	5.53 ± 0.56	11.84 ± 0.90	16.6 ± 1.7	21.5 ± 2.2
^{175}Hf	C	3.98 ± 0.39	9.62 ± 0.96	9.66 ± 0.97	12.6 ± 1.3
^{176}Ta	C	10.6 ± 1.1	13.3 ± 1.1	14.8 ± 1.5	18.7 ± 2.0
^{177}Lu	I	—	—	0.42 ± 0.05	0.33 ± 0.04
^{177m}Lu	I	0.81 ± 0.08	0.35 ± 0.04	0.33 ± 0.03	0.28 ± 0.03
^{181}Re	C	9.9 ± 1.0	10.5 ± 1.5	11.6 ± 1.0	14.9 ± 1.6
^{183}Re	I	1.47 ± 0.15	2.58 ± 0.26	2.27 ± 0.23	3.68 ± 0.37
^{183}Os	C	3.2 ± 0.3	2.62 ± 0.42	3.71 ± 0.50	3.4 ± 0.4
^{183m}Os	C	5.55 ± 0.82	7.14 ± 0.80	7.23 ± 0.80	9.36 ± 0.90
^{185}Os	C	11.7 ± 1.3	12.9 ± 1.3	13.5 ± 2.5	16.42 ± 2.50
^{185}Ir	C	—	4.01 ± 0.50	8.25 ± 0.70	8.99 ± 0.81
^{186}Ir	I	2.71 ± 0.31	2.73 ± 0.30	2.97 ± 0.30	3.13 ± 0.84
^{186}Pt	C	10.1 ± 1.1	14.7 ± 1.5	14.9 ± 1.3	21.3 ± 1.8
^{188}Pt	C	11.4 ± 1.2	11.6 ± 1.1	12.3 ± 1.3	14.9 ± 1.3
^{189}Pt	C	7.0 ± 1.0	15.0 ± 1.6	16.7 ± 2.0	19.7 ± 1.9
^{190}Ir	I	0.60 ± 0.06	0.22 ± 0.04	0.47 ± 0.05	0.64 ± 0.07
^{191}Pt	C	11.9 ± 1.2	12.4 ± 2.3	11.8 ± 2.5	16.1 ± 2.5
^{192}Hg	C	7.58 ± 0.76	9.7 ± 1.0	11.1 ± 1.1	13.9 ± 1.4
^{192}Au	I	11.5 ± 1.5	15.6 ± 4.0	19.8 ± 4.0	17.4 ± 3.1
^{193m}Hg	C	6.17 ± 0.60	7.34 ± 0.80	7.66 ± 0.74	9.47 ± 0.90
^{194}Au	I	1.31 ± 0.15	1.83 ± 0.15	2.30 ± 0.25	3.10 ± 0.20
^{195}Au	C	—	12.9 ± 1.7	19.8 ± 2.0	26.4 ± 2.7
^{195m}Hg	C	5.34 ± 0.50	6.52 ± 0.13	7.35 ± 0.80	9.20 ± 0.90
^{196}Au	I	1.13 ± 0.11	1.34 ± 0.13	1.77 ± 0.24	2.25 ± 0.25
^{197m}Hg	C	3.33 ± 0.40	3.64 ± 0.40	4.35 ± 0.40	5.71 ± 0.40
^{198m}Au	I	—	0.15 ± 0.05	$\leqslant$0.02	0.36 ± 0.04
^{198}Tl	C	10.5 ± 1.0	21.3 ± 4.1	25.1 ± 2.6	25.5 ± 4.3
^{199}Tl	C	12.5 ± 1.0	19.8 ± 2.0	21.1 ± 2.3	25.1 ± 2.5
^{200}Tl	C	20.9 ± 1.8	21.5 ± 2.3	21.5 ± 2.2	22.3 ± 1.6
^{201}Tl	I	22.4 ± 2.0	14.3 ± 1.0	13.2 ± 1.3	14.5 ± 1.5
^{201}Pb	C	8.8 ± 1.0	13.0 ± 1.3	13.2 ± 1.3	12.4 ± 1.4
^{202}Tl	C	11.0 ± 1.2	10.7 ± 1.0	11.3 ± 1.2	14.45 ± 1.50
^{203}Hg	C	0.36 ± 0.12	0.87 ± 0.09	2.57 ± 0.30	3.93 ± 0.32
^{203}Pb	I	33.12 ± 3.40	21.9 ± 3.0	28.1 ± 8.1	30.6 ± 9.4
^{203}Bi	I	1.79 ± 0.22	3.38 ± 0.43	3.1 ± 0.3	3.97 ± 0.61
^{204}Bi	I	1.62 ± 0.22	1.82 ± 0.33	2.29 ± 0.26	2.37 ± 0.30
^{205}Bi	I	2.69 ± 0.58	4.35 ± 0.76	5.8 ± 0.6	6.08 ± 0.50
^{206}Bi	I	—	1.31 ± 0.26	2.48 ± 0.31	3.37 ± 0.30

The data are summarized in table 2. As it can be noticed from table 2, there is a tendency of increasing the reaction fragment cross sections as the target mass increases for many of the included isotopes. One can suggest that, for the lighter targets, these nuclides are further away from the center of the isobaric distribution and, hence, have the smaller value of the cross

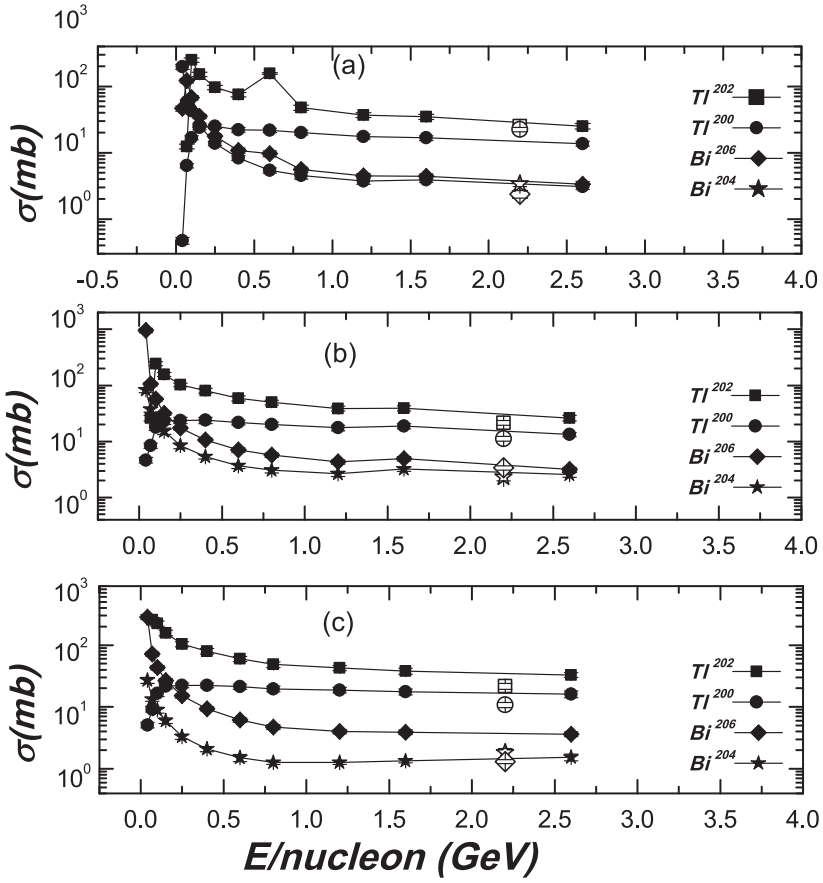

Figure 1. Cross sections for representative spallation products (indicated) from the interaction of protons in the energy range of 0.04–2.6 GeV [4] (solid symbols) together with the cross sections from the interaction of the 4.4 GeV deuterons with (a) ^{208}Pb, (b) ^{207}Pb, and (c) ^{206}Pb targets (open symbols) as a function of incident energy per nucleon (E/nucleon).

section. In the case of ^{208}Pb target, presence of the yields for both the neutron-deficient and the neutron-rich reaction fragments allows us to construct well-determined isobaric distributions with a sufficient number of fragment cross sections located along the isobaric chains. It is interesting to investigate the different reaction mechanisms which are responsible for the origin of different reaction products. Despite the absence of data on deuteron-induced reactions with lead target, we plotted (figures 1–4) together with our data for 4.4 GeV (open symbols), the excitation functions of reaction products obtained in interaction of protons with different lead isotopes in the energy range 0.04–2.6 GeV (solid symbols) [5] as a function of incident energy per nucleon (E/nucleon). The differences in excitation functions are correlated with different reaction mechanisms. In figures 1–4 we grouped the product nuclides into probable evaporation–spallation, fission and multifragmentation products in order to show the tendency of variation of nuclide production cross section with energy of incident particle ((a) for ^{208}Pb target, (b) for ^{207}Pb target, (c) for ^{206}Pb target, respectively).

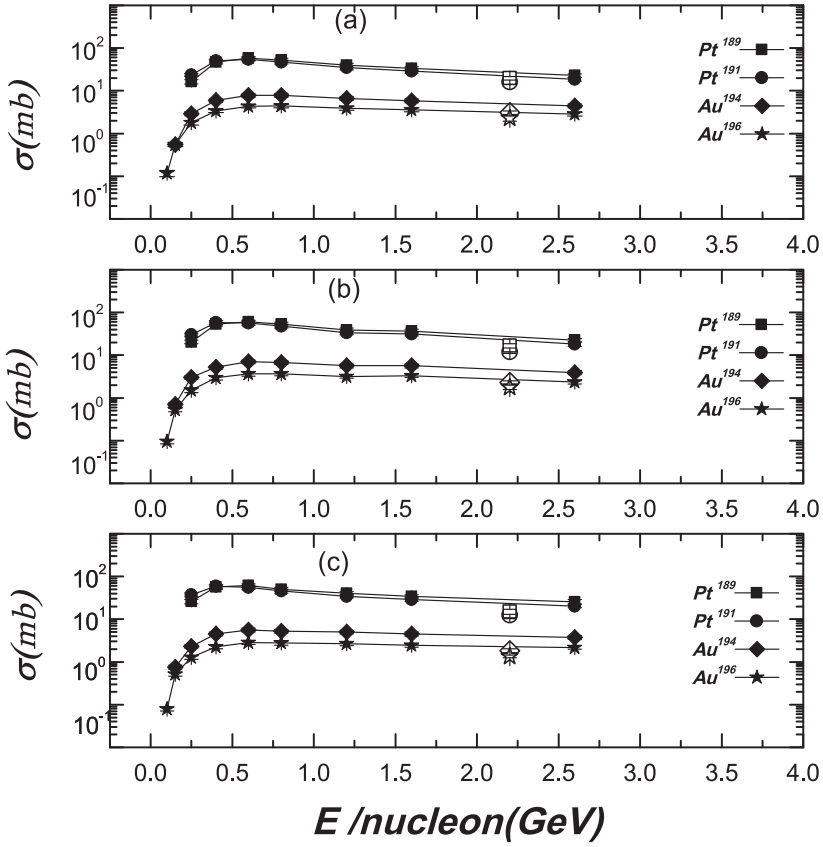

Figure 2. Cross sections for representative deep spallation products (indicated) from the interaction of protons in the energy range of 0.04–2.6 GeV [4] (solid symbols) together with cross sections from the interaction of the 4.4 GeV deuterons with (a) ^{208}Pb, (b) ^{207}Pb, and (c) ^{206}Pb targets (open symbols) as a function of incident energy per nucleon (E/nucleon).

The nuclides, whose excitation functions are shown in figure 2, are representatives of those whose mass numbers are close to the target, as examples of the simplest spallation reactions. The cross sections of these fragments are plotted as a function of incident energy per nucleon (E/nucleon).

In general, we can say that the cross sections of the formation of ^{206,204}Bi and ^{200}Tl decrease rapidly with increasing energy above an energy of 1.0 GeV, and after decrease more smoothly. The data for the reaction at 4.4 GeV fit well with the data for proton-induced reaction indicating the same mechanism of their production. The pattern seems quite similar for four nuclides presented in figure 1, especially from the target mass ^{206}Pb. Probably this is a result of the peripheral nature of such reactions, involving small energy transfer [17]. It should be noted that the changing of behavior of the ^{206}Bi and ^{202}Tl nuclides, when we considered the neutron-deficient ^{206}Pb target and the ^{208}Pb target, could be related to some isotope effect. The general trend of excitation functions of deep spallation fragments (^{194,196}Au, ^{189,191}Pt), which are shown in figure 2, is that it shows a peak in the vicinity of 0.5 GeV and the decrease from this peak with increasing energy.

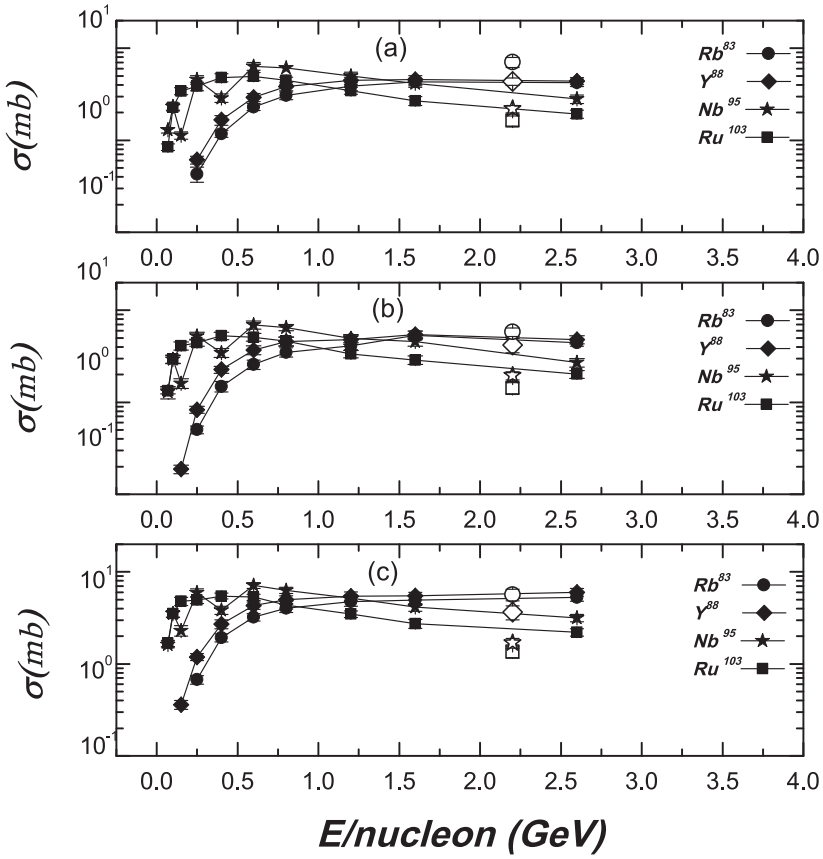

Figure 3. Cross sections for representative fission/multifragmentation products (indicated) from the interaction of protons in the energy range of 0.04–2.6 GeV [4] (solid symbols) together with cross sections from the interaction of the 4.4 GeV deuterons with the (a) ^{208}Pb, (b) ^{207}Pb, and (c) ^{206}Pb targets (open symbols) as a function of incident energy per nucleon (E/nucleon).

These trends are similar for all excitation functions for deeper spallation products with $\Delta A > 20$. The same tendency was observed in the work of Kaufman and Steinberg [18]: as it has been concluded from the experimental data of the reaction product cross sections that ranged from 100 MeV up to even more than 10 GeV proton energy, the excitation functions of nuclides close to the target have a maximum value at lower energies, decrease with further increasing energy and reach asymptotic values at the high-energy limit. We can also mention the similarity of the behavior in the case of deep-spallation reaction products with those of [18], where the excitation functions of the fragments show peaks around incident energy 200–600 MeV, decreasing up to energy 6 GeV and then become constant above this energy limit. Moreover, from the data of [18], we can see that there is a general trend for the excitation functions of spallation–evaporation fragments: with increasing mass loss from the target, the maximum cross section decreases and the bombarding energy above which the cross section is constant also increases with the mass loss.

The excitation functions of medium-mass fragments, such as ^{103}Ru, ^{95}Nb, ^{88}Y and ^{83}Rb, presented in figure 3, differ from those of the spallation and deep spallation nuclides (figures 1

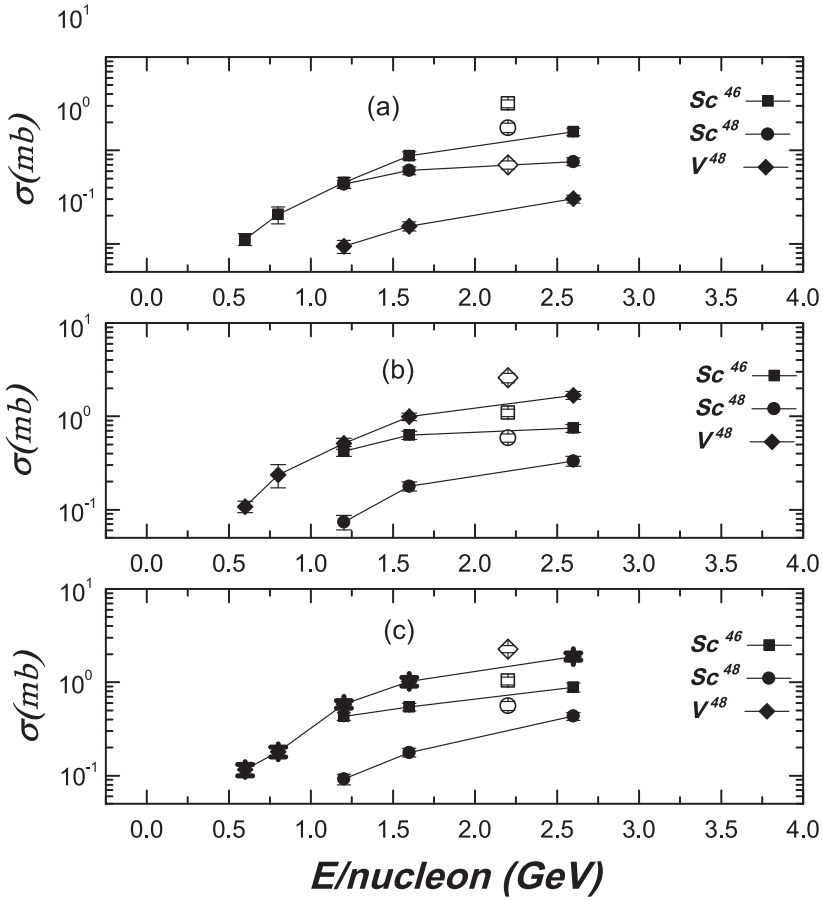

Figure 4. Cross sections for representative multifragmentation products (indicated) from the interaction of protons in the energy range of 0.04–2.6 GeV [4] (solid symbols) together with cross sections from the interaction of the 4.4 GeV deuterons with (a) ^{208}Pb, (b) ^{207}Pb, and (c) ^{206}Pb targets (open symbols) as a function of incident energy per nucleon (E/nucleon).

and 2). The difference is due to the different contributions of deep spallation, fission and multifragmentation. The initial rise in cross section is quite steep for these nuclides, indicating the importance of high deposition energies in their formation. Starting from energy 0.8 GeV one can see the sharp decrease of excitation functions with energy increase for ^{103}Ru, ^{95}Nb nuclides, almost constant value of cross section in the case of ^{88}Y isotope. The high value of the production cross section in the case of ^{83}Rb can be explained as following: such nuclide is a neutron-deficient, and it, probably, has more contribution of multifragmentation than the other nuclides. The pattern can be understood as the coexistence of different decay modes involved in the formation of reaction residues. It should be noted that the contribution of the different reaction channels, namely, multifragmentation and deep spallation, has been discussed in [18] for this medium mass range of the reaction fragments. The authors indicated the change in the reaction mechanisms by observing the sharp rise of the excitation function for the neutron-deficient medium-mass nuclides at lower energy range, and the peak value of the cross section for the neutron-excess nuclides, formed probably by binary fission in the

range of 300–500 MeV, with further fall off before reaching the asymptotic behavior at high energies.

The excitation functions for some light nuclides, ^{46,48}Sc and ^{48}V, which are generally termed as multifragmentation products are shown in figure 4. Actually, we cannot clearly isolate the fission process from the multifragmentation, and both processes overlap. As has been shown in recent work of Napolitani *et al* [19], in the vicinity of the multifragmentation threshold, both the fission and the multifragmentation processes can contribute to the formation of these products. One can see from figure 4 a monotonic and sharp rising excitation function up to the energy 2.6 GeV. The possible production of these fragments has been discussed in [1]. It was found that in the so-called transition energy regime, at excitation energy of the hot composite system more than 3–4 MeV per nucleon, the multifragmentation process starts to compete with fission and contributes appreciably to the production cross section. The investigation of the excitation function for some light nuclides, done in [18], showed the same sharp rising of cross section with further monotonic increase to the asymptotic value, as it was observed in the present data, without any peak and subsequent fall off of the latter.

A question of relevance concerning the mechanism(s) of energy transfer in relativistic nucleus–nucleus collisions is the question of whether the energy transfer scales as the total projectile kinetic energy or as the energy per nucleon of the projectile. In this regard, it is interesting to compare our results with similar results from the interaction of high energy protons. In figure 5, we show a comparison between the target fragment cross sections for the reaction of 4.4 GeV deuterons ((a) for ^{208}Pb target, (b) for ^{207}Pb target, (c) for ^{206}Pb target, respectively), and similar measurements for the same products from the reaction of 2.6 GeV protons with ^{206,207,208}Pb [4]. The points represent the ratios of individual cross sections. As one can see in figure 5, the cross sections for the heavier mass fragments $A > 130$ (fragments formed by the evaporation process) are lower than those for proton-induced reactions. Namely, the ratios of cross section ratios are equal for the ^{208}Pb, ^{207}Pb and ^{206}Pb targets, respectively, 0.8 ± 0.1, 0.7 ± 0.1 and 0.54 ± 0.08. This fact is confirmed by the observations in figures 1 and 2 that the cross section for evaporation–spallation products decreases with increasing the bombardment energy.

Formation of these nuclides would correspond to a peripheral collision with large impact parameter and low excitation energy. One can see from figure 5 that in the mass range $60 \leqslant A \leqslant 130$, wherein we can expect the domination of the fission fragment production and partly contribution of the multifragmentation process, the cross sections are almost similar within uncertainties of determination for proton- and deuteron-induced reactions.

The cross section ratios for this mass range are 1.36 ± 0.20, 1.14 ± 0.17 and 0.9 ± 0.1 for the ^{208}Pb, ^{207}Pb and ^{206}Pb targets, correspondingly. In this mass range the competing processes, such as fission, multifragmentation and evaporation vary with the mass of the cold residue. A similar effect was pointed out in [9] for deuteron- and proton-induced reactions on a lead target. One can also see from figure 5 that a depletion of spallation–evaporation production is compensated by a larger production from the multifragmentation process [1].

The enhanced cross sections of the lighter products ($A < 60$) in the deuteron-induced reaction have been interpreted in the terms of changing the reaction mechanisms, namely, by a larger contribution from the multifragmentation process compared to the fission. In this mass range the cross section ratios were found to be equal 1.96 ± 0.30, 1.47 ± 0.22 and 1.2 ± 0.2 for the ^{208}Pb, ^{207}Pb and ^{206}Pb targets, respectively. Enhanced cross sections of light fragments have been previously reported for the reactions in different targets induced by different projectiles at high energies of incident particles [11, 20, 21]. The enhanced emission of light fragments thus appears to be a general feature of relativistic particle-induced reactions

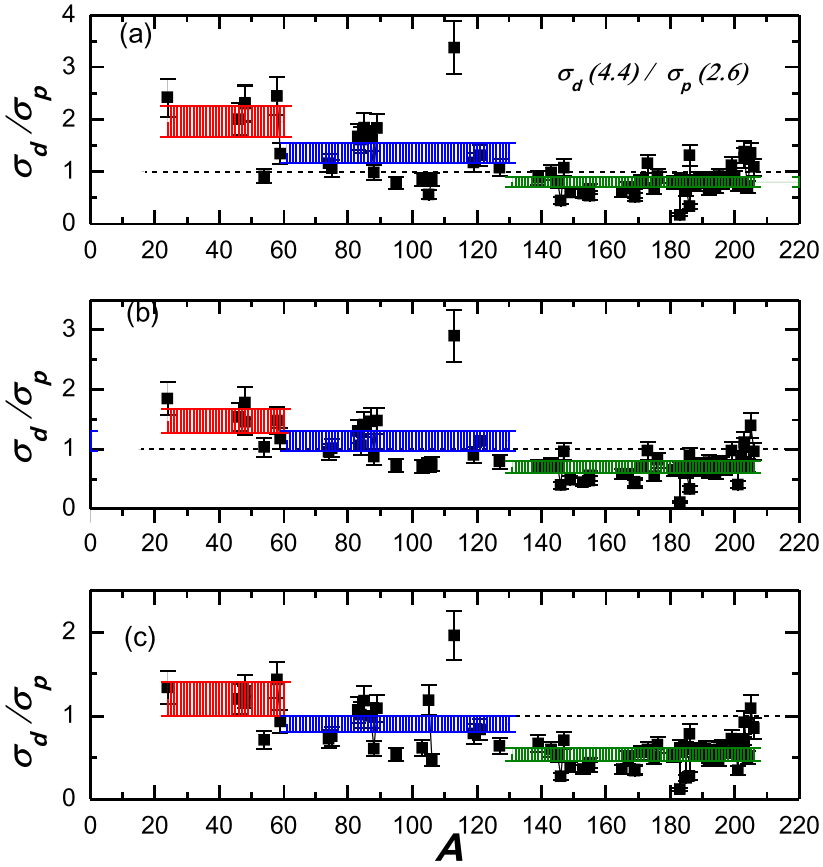

Figure 5. Cross section ratios, σ_d/σ_p, of target residues from the 4.4 GeV deuteron-induced reactions of present work and 2.6 GeV protons from [4] with (a) ^{208}Pb, (b) ^{207}Pb, and (c) ^{206}Pb targets. The average ratios of the fragment cross sections and their uncertainties, corresponding to the different mass regions are indicated as following: $A < 60$ (red shaded area), $60 \leqslant A \leqslant 130$ (blue shaded area) and $A > 130$ (green shaded area).

and is indicative of the importance of interactions in which high excitation energies are transferred to the struck nucleus. According to the theoretical calculations of Cugnon in [22] for the high-energy domain of the projectile, the average excitation energy at the end of the cascade stage generated by the deuterons of 4 GeV total incident energy on ^{208}Pb target is twice higher than the average excitation energy in the case of 2 GeV proton-induced reaction. Such high energy deposit is consistent with the results in figure 5 of the present work, namely, an enhanced production of the lighter groups of fragments in the more energetic reactions with deuterons. In figure 5, the average ratios of the fragment cross sections and their uncertainties, corresponding to the different mass regions indicated by red, blue and green shaded areas are shown for the fragment mass regions $A < 60$, $60 \leqslant A \leqslant 130$ and $A > 130$, respectively. As it is apparent from figure 5, in the mass range of the reaction fragments $A < 60$ the average ratio of the fragment cross sections is higher than the corresponding ratio for the other mass ranges. Hence, in the mass range $A < 60$ one can expect a two-nucleon interaction mechanism of the deuteron with the target nucleus. On the other hand, in the mass

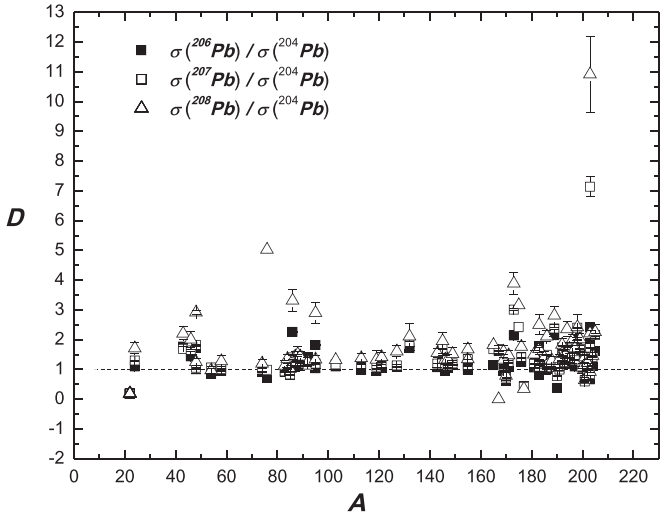

Figure 6. Cross section ratios, $D = \sigma(^{206,207,208}Pb)/\sigma(^{204}Pb)$, of target residues from the 4.4 GeV deuteron-induced reactions of present work.

range $60 \leqslant A \leqslant 130$ and $A > 130$, the cross section ratios, σ_d/σ_p, are about unity or even less. This fact can indicate that during the formation of the fragments due to the spallation or/and fission processes, not necessarily the two nucleons of the deuteron participate. For the fragments from $A = 24$ to 206, the average ratio of the mass yield for producing a given fragment in these reactions compared to the proton-induced reaction (figure 5) are 1.1 ± 0.2, 0.9 ± 0.2 and 0.7 ± 0.1 in case of the ^{208}Pb, ^{207}Pb and^{206}Pb targets, respectively. Comparison of the production cross section ratio from the present study and those produced by high energy protons [4] shows agreement for targets ^{208}Pb, ^{207}Pb within the accuracy of measurements at approximately the same value of projectile kinetic energy per nucleon instead of being about twice as large. This fact may be due to the absence of additional interaction of the two nucleons of the deuteron with the target nucleus and the similarity of the interactions of protons and deuterons. In figure 6, the fragment cross section ratios from ^{206,207,208}Pb targets and the corresponding cross sections from ^{204}Pb target, D, are presented as a function of the fragment mass number A. As can be seen from figure 6, the production cross sections of the three targets for the current experiment increase with increasing target mass number. In the study performed in [4] the cross sections do not manifest such a tendency, and in most of cases the cross sections of fragments are larger for ^{206}Pb than for ^{207}Pb.

To obtain the cross section for each isobar it is necessary to estimate cross sections of isotopes not measurable by the induced-activity method. These cross sections can be obtained by considering the charge distribution for each isobar, i.e. using the independent cross sections for each element of an isobar chain as a function of Z.

In the present work the charge distribution of each isobar chain was assumed to be expressed by the following form from [18]:

$$\sigma(Z, A) = \sigma(Z_p, A)\exp(-R\,|Z - SA + TA^2|^{3/2}), \tag{3}$$

where $\sigma(Z, A)$ is the independent production cross section for a given nuclide with atomic charge Z and a mass number A; $\sigma(Z_p, A)$ is the maximum value of the distribution obtained when the argument of the exponential function is zero, and the parameters R, S and T are the

free parameters in the fitting procedure. The parameters S and T define the most probable charge Z_p for a given isobar chain A, which is not necessarily an integer. The parameter R is related to the width of the charge distribution. As it was reported earlier in [23, 24], the width of the charge distribution is practically independent of the excitation energy and of the nuclear properties of the projectile and target. On the base of the value of $\sigma(Z_p, A)$ in equation (3), the total isobaric cross section of the mass chain A, $\sigma(A)$, then has been calculated. At first, only independent cross sections (I) were used in the fitting of the charge distributions. Hence, during the successive approximation procedures, the estimation of the independent component of cumulative cross section could be extracted. In this work we obtained mass dependent expression for R given by $R = 30\,A^{-0.79}$ for all targets under study and in the whole mass range of the reaction products. In order to uniquely specify the variables R, S and T one would need to measure four independent yield cross sections for each isobar. In fact, the nature of radioanalytical studies such as the one applied here does not, in general, lend itself to the measurement of isobaric members. Rather, a wide assortment of radioactivities are observed which span the entire range of the periodic table that is accessible in the nuclear reaction. As a result relatively few isobaric pairs are observed. Here, we adopted the assumption that the charge distribution curves for neighboring isobaric chains should be similar; thus radionuclide cross sections from a limited mass range can be used to determine a single charge distribution curve. In the case of shortage of the experimental data on the independent cross sections we can use the fact that the charge distribution should be similar for neighboring isobaric chains as observed previously in different studies [23, 24]. The validity of this assumption in the case of ^{208}Pb target mass is tested in figures 7(a), (b) and (c) by plotting the fractional cross sections (the ratio of the production cross section of a fragment to the total cross section of the corresponding mass chain) as a function of the difference $(Z - Z_p)$ for some group of masses, where each mass chain would have a specific Z_p. A function given by equation (3) was used to fit the corresponding charge distributions for the indicated mass ranges.

During the fitting procedure it was found that the value of $R = 30\,A^{-0.79}$ was unchanged for all targets under study in the whole mass range of the reaction products. This means that the width of the charge distribution for given mass number is the same for all range of product mass number A. The parameter S was found to be 0.47 for all targets and reaction products in the mass range $A < 130$, and it was equal to 0.49 for products with masses $A \geqslant 130$. The parameter T was larger for the heavier fragments: the values of T for mass range $A < 130$ were 2.7×10^{-4}, 2.8×10^{-4}, 2.9×10^{-4} and 3.0×10^{-4} in the case of ^{204}Pb, ^{206}Pb, ^{207}Pb, and ^{208}Pb, respectively. For the mass range $A \geqslant 130$ the values of T parameter were 3.7×10^{-4}, 3.8×10^{-4}, 3.9×10^{-4} and 4.0×10^{-4} in the case of ^{204}Pb, ^{206}Pb, ^{207}Pb, and ^{208}Pb, respectively. These values suggest that there are more neutron-deficient nuclei for lighter mass range ($A < 130$), and more neutron-rich nuclei for the heavier mass range ($A \geqslant 130$), which are more related to the spallation–evaporation nuclides. Such displacement can be directly linked to the excitation energy of the reaction residues.

As it was noted in [25], at sufficiently large excitation energies, independent of the assumed Z and A of the primary fragments, the nucleon evaporation results in that the average location of the secondary fragments in the chart of nuclide is always close to a particular line (Evaporation Attractor Line—EAL). The location of this line is mainly determined by the competition between proton and neutron evaporation. The products of this process can therefore be understood as the evaporation residues associated with the decay of highly excited primary fragments produced by the initial reaction. For the excited composite system on the neutron-rich side of the line, neutron emission is the most important evaporation mode and this drives the system towards the line. On the neutron-poor side, proton emission is the

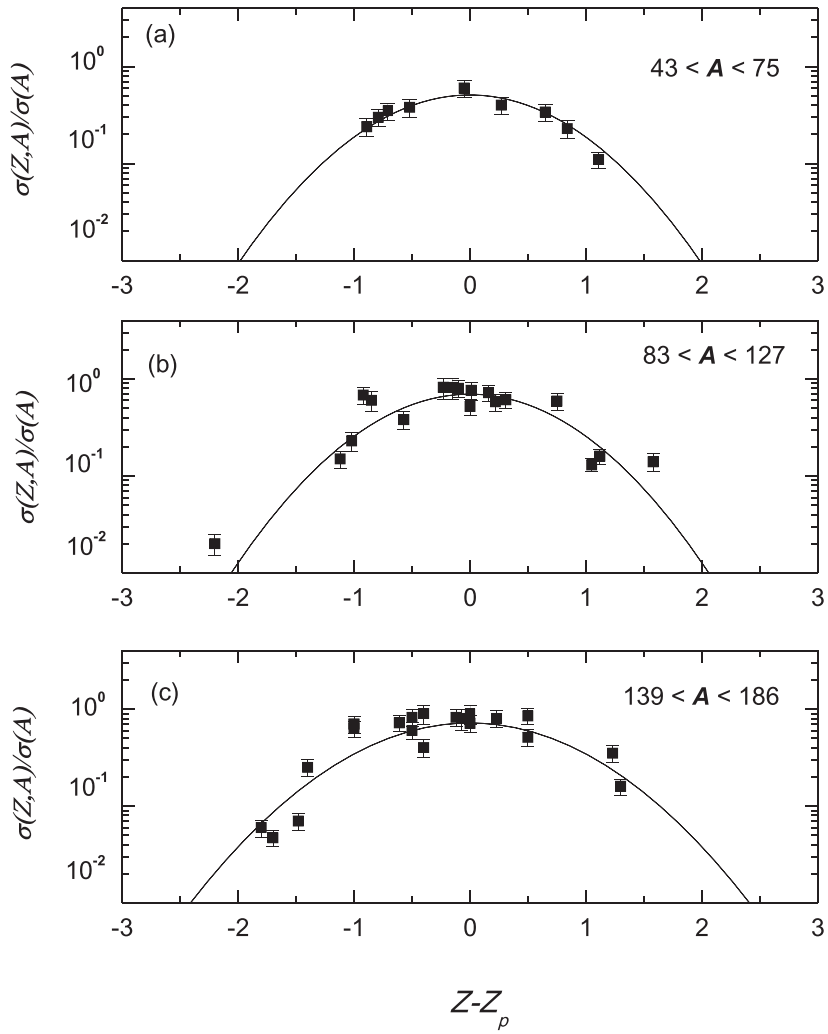

Figure 7. The fractional cross sections (cross section of fragment production to total cross section for given mass number) for different isobaric chains in the mass range indicated as a function of (Z–Z_p) for the 4.4 GeV deuteron-induced reaction on ^{208}Pb. The solid line is the corresponding charge distribution.

strongest decay mode and again, this acts to move the decaying system towards the line. According to the [25] the obtained evaporation attractor line can be well approximated by the following expression: $Z = 0.909 \times N - 1.12 \times 10^{-3}N^2$.

We used the prediction of EAL in order to see the deviations of the most probable charge from the calculations, giving the average location of the fragmentation products produced in the reaction of 4.4 GeV deuterons on target nuclei located close to the line of β-stability. The results of comparison are demonstrated in figures 8(a), (b), 9(a), (b) for the ^{204}Pb, ^{206}Pb, ^{207}Pb, and ^{208}Pb targets, respectively, where the dependence of the average atomic number is a function of neutron number for the observed nuclide. In figures 8(a), (b), 9(a), (b) line signed by the crosses corresponds to the *EAL* prediction, the solid black line corresponds to the stable nuclei, the dotted line is for Z_p for $A < 130$, the dashed line is Z_p for $A \geqslant 130$, the open black

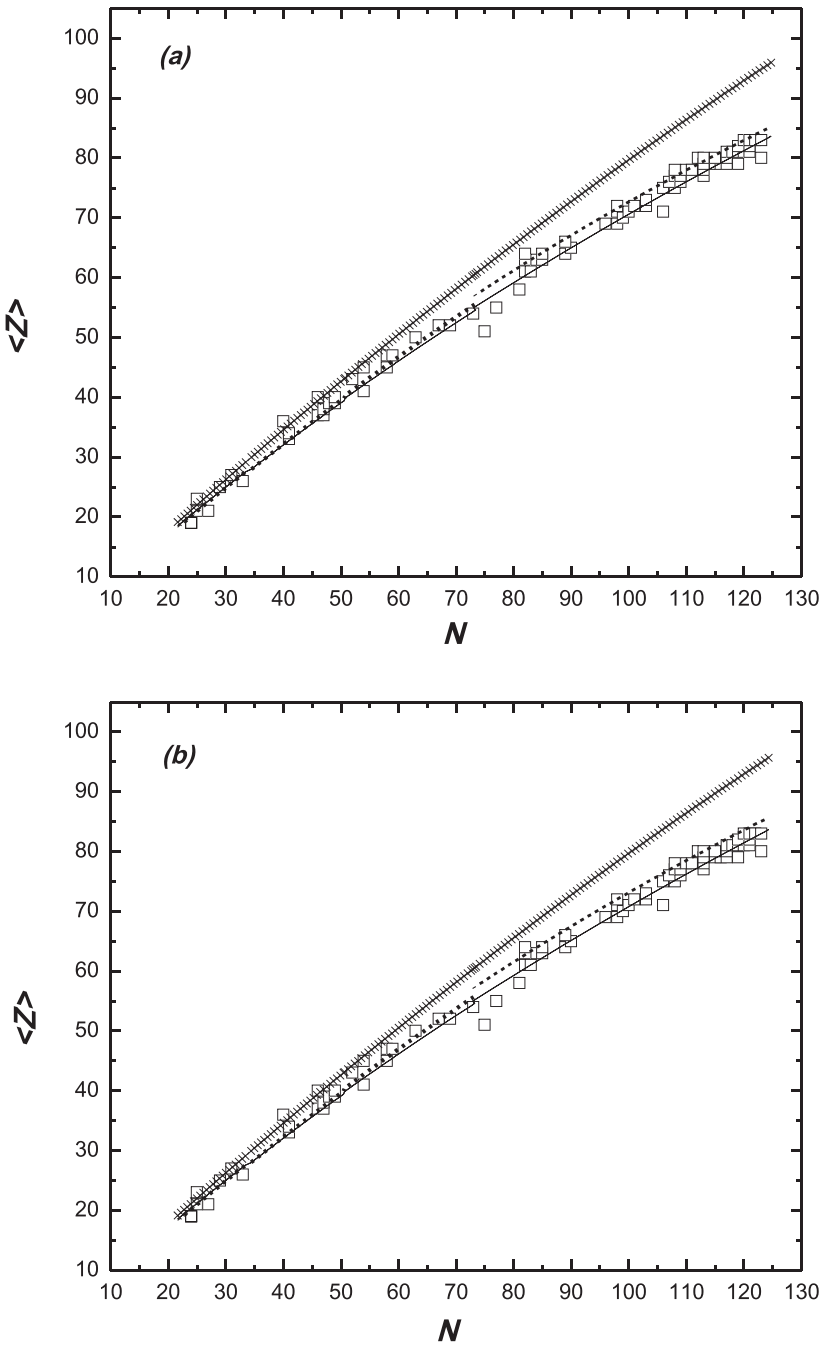

Figure 8. Average atomic number as a function of neutron number for the observed nuclide. The line signed by the crosses is the EAL prediction, the solid black line corresponds to the stable nuclei, the dotted line is for Z_p for $A < 130$, the dashed line is Z_p for $A \geqslant 130$, the open black squares refer to the reaction residues of the present paper: (a) for the ^{208}Pb, (b) for the ^{207}Pb targets, respectively.

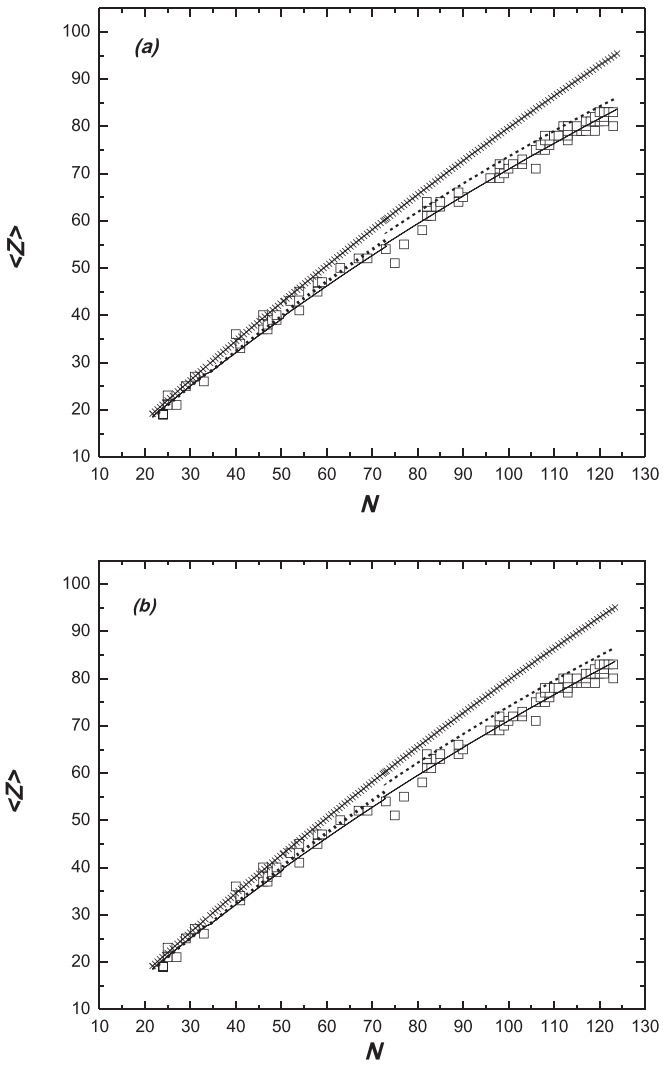

Figure 9. The same as in figure 8: (a) for the ^{206}Pb, (b) for the ^{204}Pb targets, respectively.

squares refer to the reaction residues of the present paper. As one can see in figures 8 and 9, decaying fragments with masses $A < 130$ approach and almost reach the *EAL*, the displacement between Z_p and Z_{EAL} for such mass region in the interval varies from less than one mass unit up to 4–5 u. Residues with $A < 130$ are highly excited, which has been confirmed by our recent study of the kinematics properties of the reaction residues [17]. According to [25], as the nuclear temperature rises, the difference between the energies required to remove a proton and to remove a neutron becomes less important and so the rates for proton and neutron emission become more similar, on average; an equal number of protons and neutrons are lost and the system retains a memory of its degree of neutron or proton richness. The fragments with $A \geqslant 130$ are connected to the spallation–evaporation process during the cooling mechanism of the cascade remnant. They have a considerably low excitation energy

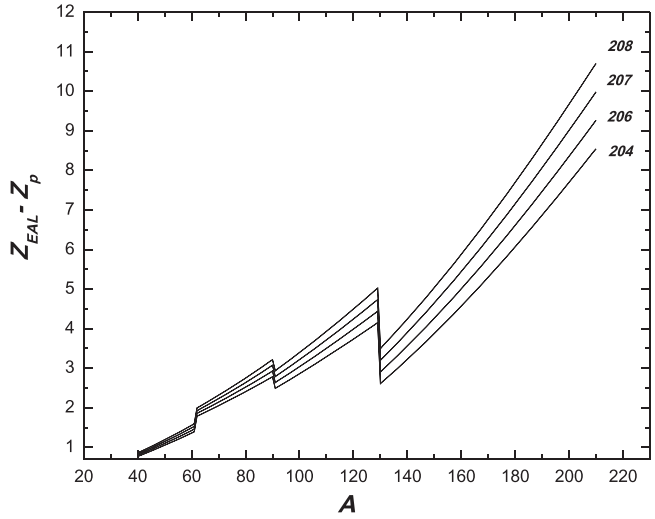

Figure 10. The deviation of the most probable charge, Z_p, from that prediction of the EAL, Z_{EAL}, for the ^{208}Pb, ^{207}Pb, ^{206}Pb, and ^{204}Pb targets versus nuclide mass number A.

and a large impact parameter [17]. The displacement of these nuclei from the Z_{EAL} values varies in the 3–11 mass units range. As it was noted in [25] for the neutron-rich system, the average position of the secondary fragments never reaches the evaporation attractor line. The appreciable effect is an overall tiny displacement towards the neutron-poor side due to evaporation, hence, the low-energy reaction fragments locate far from the attractor line. The general tendency for all reaction residues is that the variation between the most probable charge Z_p and Z_{EAL} increases when it ranges from target mass 204 to 208. This effect can be clearly seen in figure 10, where we present the deviations of Z_p from Z_{EAL} for all target masses versus nuclide mass number A. As can be seen from figure 10, the slope of the solid lines, that represents each target mass, becomes steeper when moving from light fragments to heavier ones and from the lighter ^{204}Pb target to the heavier ^{208}Pb target.

In our experiment, low-energy excited residues with $A \geqslant 130$ and residues with $A < 130$ but higher excitation energy were produced. This fact is confirmed by our recent study of the kinematics properties of the reaction residues from the gold target irradiated by deuterons at 4.4 GeV [17]. Another observation that the parameter T increases with increment of the mass of the target caused by the nuclear composition of the irradiated targets: the higher the number of the target neutrons, the higher the evaporation is, during the de-excitation stage of the reaction.

Using the values R, S, T and the equation (3), the total isobaric cross sections $\sigma(A)$ were calculated by fitting the experimental data. These cross sections are shown as the solid squares in figures 11–14 for the ^{204}Pb, ^{206}Pb, ^{207}Pb, and ^{208}Pb targets. The measured cross sections of ^{22}Na and ^{24}Na have been added in figures 11–14 instead of integrated yields for these mass numbers. All other representatives for these mass chains are either stable or very short-lived isotopes, thus cannot be detected by induced-activity method used in this work. The distribution of products observed in the high-energy nuclear reactions is currently explained in the terms of appropriate combinations of the following processes: the initial high-energy cascade; the evaporation of nucleons and other more complex particles from excited nuclei: fission, spallation and multifragmentation. The mass-yield distributions

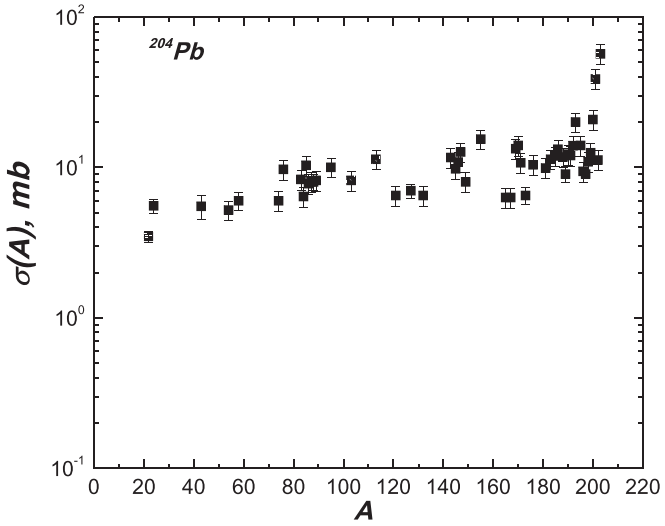

Figure 11. Mass-yield distribution for the isobars produced by the 4.4 GeV deuteron-induced reactions on the ^{204}Pb target. Solid squares are the estimated isobaric cross sections from the present work.

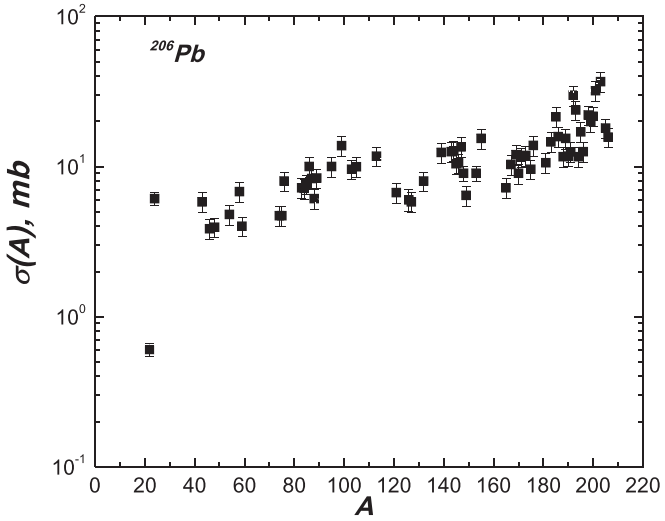

Figure 12. Mass-yield distribution for the isobars produced by the 4.4 GeV deuteron-induced reactions on the ^{206}Pb target. Solid squares are the estimated isobaric cross sections from the present work.

display the common features. First of all, the cross sections decrease sharply with decreasing mass A in the vicinity of the target mass. Products in this mass region result from the most peripheral interactions, in which few nucleons are knocked out of the target and little energy transfer occurs. This is the mass region where evaporation–spallation is the dominant mechanism.

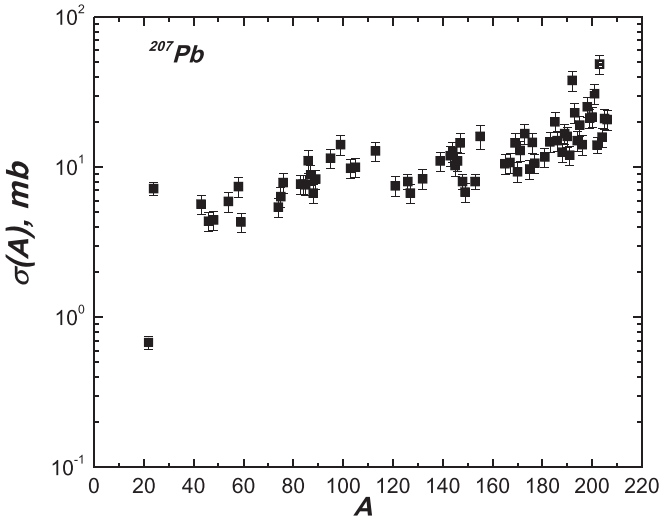

Figure 13. Mass-yield distribution for the isobars produced by the 4.4 GeV deuteron-induced reactions on the ^{207}Pb target. Solid squares are the estimated isobaric cross sections from the present work.

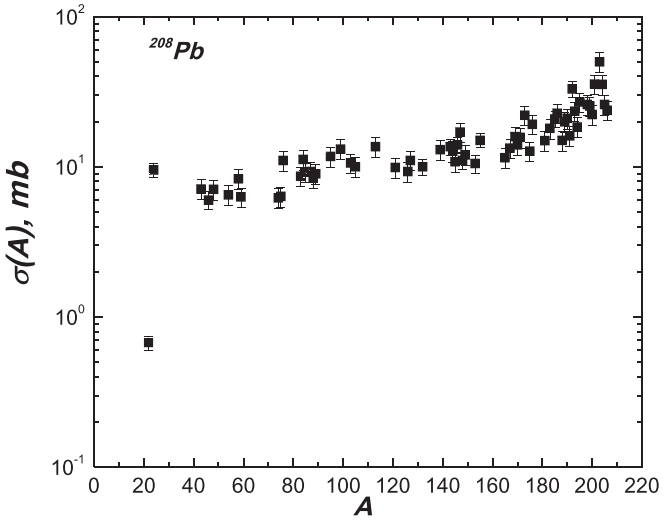

Figure 14. Mass-yield distribution for the isobars produced by the 4.4 GeV deuteron-induced reactions on the ^{208}Pb target. Solid squares are the estimated isobaric cross sections from the present work.

From figures 11–14 a special zone of products can be distinguished just below the evaporation–spallation region. Such a zone arises from high-energy fission. Although there is almost no clear-cut distinction between evaporation–spallation and fission, one can see in figures 11–14 the evident fission peak in the mass yield-curve at about half the target mass ($A \sim 100$) [4, 5]. Therefore, the total mass-yield distribution can be described as the sum of a broad evaporation–spallation distribution and the distribution in the so-called 'fission' mass

Table 3. Total inelastic cross sections ($\sigma_{\rm tot}$) estimated by the Glauber model calculation for the interaction of 4.4 GeV deuterons with lead isotopes targets.

Target	$\sigma_{\rm tot}$ (Glauber) (b)
^{204}Pb	2.023
^{206}Pb	2.035
^{207}Pb	2.041
^{208}Pb	2.047

region. Then the two distributions overlap extensively and the division of the mass-yield distribution into zones can be rather arbitrary. However, to confirm the presence of fission as an additional important process contributing to the reaction products requires detailed model calculations. As it has been shown in the work of Viola *et al* [26] for the reaction $p + Au$ at 10.2 GeV/c, the production cross section in the mass range smaller than $A = 60$ is eventually increased with decreasing A, which can be connected with the rising contribution of the multifragmentation process [1, 19].

In table 3 one can see the values of the total inelastic cross sections for ^{204}Pb, ^{206}Pb, ^{207}Pb, and ^{208}Pb targets estimated within the classic Glauber model given in [27].

$$\sigma_{dA}^{\rm inel} = \int {\rm d}^2 b[1 - \exp(-\sigma_{dN}^{\rm tot} \int_{-\infty}^{\infty} \rho(\mathbf{b}, z){\rm d}z)], \tag{4}$$

where $\rho(b, z)dz$ is one particle nuclear density, $\sigma_{dN}^{\rm tot}$ is the interaction cross section of the incident deuteron with the nucleon in the nucleus and the Fermi parametrization was used for $\rho(r)$ with parameters from [28].

However, due to the limitation caused by the registration and measurement methods used in the present experiment, which did not allow us to extract the cross section for each process under study (fragmentation, fission, and evaporation–spallation) from the reaction mass-yield distribution, we could not deduce the value of the experimental total reaction cross section. It can also be noticed that the interaction of high-energy particles with nuclei leads to a very rich spectrum of phenomena and can be understood and described theoretically. On the other side, the production cross sections have a great importance for models and code improvements. Therefore, the work should be continued in the future in order to allow benchmarking of newly developed models.

4. Conclusion

Production cross sections for the formation of target fragments were determined from the interaction of 4.4 GeV deuterons on isotopically enriched lead targets. These elements were identified by measuring the intensities of their γ-ray decays by high-resolution HpGe spectroscopy. From the individual production cross sections charge- and mass-yield distributions were determined. The charge distributions were analyzed in terms of a 3-parameter equation. The charge distributions have shown some contribution of neutron-deficient nuclei for mass chains heavier than $A = 130$, where more neutron-rich nuclei are expected to be formed. It was suggested that such displacement could be directly linked to the excitation energy of the reaction residues. The total inelastic cross sections for 4.4 GeV deuterons were estimated within the Glauber model calculation. Production cross section ratios of the present paper and those produced by high-energy protons show good agreement for the ^{208}Pb and ^{207}Pb targets, within the accuracy of measurements and at approximately the same projectile

kinetic energy per nucleon. The analysis of excitation functions for different fragments, including data of 0.04–2.6 GeV proton-induced reaction and for 4.4 GeV deuteron-induced reaction of the present work, suggests the coexistence of the different decay modes in the formation of the reaction residues, such as spallation, fission and multifragmentation.

Acknowledgments

The author GSK would like to thank the São Paulo Research Foundation (FAPESP—grant 2018/19943–6) for the partial financial support. The author VG would like to thank the São Paulo Research Foundation (FAPESP—grant 2016/02863–4) and the Conselho Nacional de Desenvolvimento Cientifico (CNPq—grant 302969/2013–6) for financial support. Authors are grateful to technical personnel of the Nuclotron for providing reliable operation of the Nuclotron and the main part of the experimental installation.

ORCID iDs

S V Gaginyan https://orcid.org/0000-0001-6319-9895
A Deppman https://orcid.org/0000-0001-9179-6363

References

[1] Borderie B and Rivet M F 2008 *Prog. Part. Nucl. Phys.* **61** 551
[2] Pouthas J *et al* 1995 *Nucl. Instrum. Meth.* A **357** 418
[3] Adam J *et al* 2005 *Eur. Phys. J.* A **23** 61
Mukaiyama T *et al* 2002 *Prog. Nucl. Energy* **40** 403–13
[4] Titarenko Y E 2009 *IAEA Nuclear Data Section* INDC(CCP)-0447 Vienna International Centre, A-1400, Vienna, Austria
[5] Titarenko Y E *et al* 2002 *Phys. Rev.* C **65** 064610
[6] Prokofiev A V 2001 *Nucl. Instrum. Meth.* A **463** 557
[7] Rahimi F *et al* 1973 *Phys. Rev.* C **8** 1500
[8] Kelic A *et al* 2004 *Phys. Rev.* C **70** 064608
[9] Enqvist T *et al* 2002 *Nucl. Phys.* A **703** 435
[10] Wallenius J 2019 *Annals Nucl. Energy* **125** 74
[11] Balabekyan A *et al* 2014 *Phys. Rev.* C **90** 054612
[12] Bradt H C and Peters B 1950 *Phys. Rev.* **77** 54
[13] Banaigs J *et al* 1971 *Nucl. Instrum. Meth.* A **95** 307
[14] Frána J 2003 *J. Radioanal. Nucl. Chem.* **257** 583
[15] Firestone R B 1998 *Tables of Isotopes* 1998 Update (with CD ROM) ed S Y Frank Chu and C M Baglin 8th edn (New York: Wiley Interscience) (CD-ROM editor)
[16] Karapetyan G 2015 *Eur. Phys. J. Plus* **130** 180
[17] Balabekyan A *et al* 2014 *Phys. Rev.* C **89** 054604
[18] Kaufman S B and Steinberg E P 1980 *Phys. Rev.* C **22** 167
[19] Napolitani P, Schmidt K-H and Tassan-Got L 2011 *J. Phys. G: Nucl. Part. Phys.* **38** 115006
[20] Porile N T, Cole G D and Rudy C R 1979 *Phys. Rev.* C **19** 2288
[21] Sullivan J D, Price P B, Crawford H J and Whitehead M 1973 *Phys. Rev. Lett.* **30** 136
[22] Cugnon J, Volant C and Vuillier S 1997 *Nucl. Phys.* A **625** 729
[23] Kudo H *et al* 1998 *Phys. Rev.* C **57** 178
[24] Branquihno C L and Robinson V J 1977 *J. Inorg. Nucl. Chem.* **39** 921
[25] Charity R J 1998 *Phys. Rev.* C **58** 1073
[26] Viola V E *et al* 2006 *Phys. Rep.* **434** 1
[27] Glauber R J 1970 *High Energy Physics and Nuclear Structure* (New York: Plenum Press)
[28] Murthy P V R *et al* 1975 *Nucl. Phys.* B **92** 269